GRAIN SEGMENTATION OF MULTI-ANGLE PETROGRAPHIC THIN SECTION MICROSCOPIC IMAGES

Feng Jiang[⋆†], *Qing Gu*[⋆], *Huizhen Hao*[⋆], *Na Li*[⋆]

[⋆]State Key Laboratory for Novel Software Technology (Nanjing University), Nanjing 210023, China
[†]College of Mobile Internet, Taizhou Institute of Sci. & Tech., NUST, Taizhou 225300, China

ABSTRACT

Grain segmentation of petrographic thin section microscopic (TSM) images is the first step for computer aided mineral identification and rock naming. The TSM images contain a large number of mineral grains and the differences among adjacent grains are usually ambiguous, which makes current segmentation technologies inefficient. In this paper, we take advantage of multi-angle TSM images and propose a method for grain segmentation. Accordingly, the method consists of two steps, in the first step, we enhance the SLIC algorithm to handle multi-angle images and produce the initial superpixels. In the second step, multiple features are extracted for comprehensive description of the superpixels, and dissimilarities between superpixels are measured according to the extracted features. Then the multi-angle region merging algorithm is employed to merge similar adjacent superpixels and get the final segmentation results. Experimental results demonstrate both the effectiveness and potential of the proposed method for grain segmentation of TSM images.

Index Terms— Thin section microscopic images, image segmentation, multi-angle images, superpixel

1. INTRODUCTION

Grain segmentation of petrographic thin section microscopic (TSM) images is a primary step in petrology including mineral identification and rock naming. TSM images can be plane-polarized images or cross-polarized images [1]. Unlike plane-polarized images, adjacent grains in cross-polarized images produce different interference colors by cross-polarized light from different orientations [2]. We call these the multi-angle TSM images. For example, in Fig.1 (b), the regions r_1 and r_2 are similar and may be misread as the same grain, but in Fig.1 (a)(c), the two regions are easily distinguishable from different angles.

Currently, geologists have to conduct manual segmentation on TSM images, which is tedious, time-consuming and subject to individual experiences. In principle, any existing image segmentation method can be used to automate the grain segmentation, such as region growing [3] [4], graph cuts [5], Quickshift [6], TurboPixel [7], ERS [8], SEEDS [9], LSC [10] and SLIC [11]. However, these methods are generally designed for ordinary images and may not be appropriate for grain segmentation of TSM images which contains hundreds of mineral grains, while the background is hardly recognizable. In addition, as shown in Fig.1, the multi-angle TSM images can help overcome the blurring effects and achieve more accurate grain segmentation than using singular image.

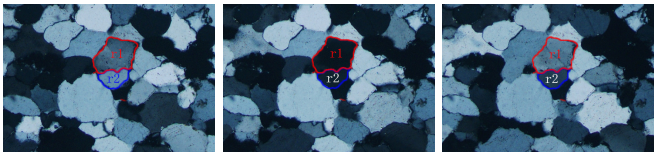

(a) orientation=15° (b) orientation=30° (c) orientation=45°

Fig. 1: Multi-angle TSM images

In this paper, we take advantage of multi-angle TSM images, and put forward a two step grain segmentation method. Our contributions include the follows: (1) The SLIC algorithm is enhanced for multi-angle images to overcome the blurring effects when generating suitable superpixels. (2) Multiple features are combined to characterize the superpixels and compute the dissimilarity measure among the superpixels. (3) A multi-angle region merging algorithm is designed to combine the superpixels to final grains. We compare the method with documented segmentation technologies, and the results demonstrate the effectiveness and potential of the method.

2. OUR METHOD

Our method contains two steps, as illustrated in Fig.2. Given the multi-angle TSM images, multi-angle SLIC is firstly applied to generate superpixels. Secondly, multiple features are extracted to measure the degree of dissimilarity among superpixels. The superpixels with low degree of dissimilarity are merged to obtain the final segmentation results.

2.1. Some Notations

Given an image with N pixels, and let P contain its pixels. The image is denoted by $\mathbf{X} = \{\mathbf{x}_p\}_{p \in P}$, where $\mathbf{x}_p$ stands for a pixel. Each $\mathbf{x}_p$ can be represented as a feature vector

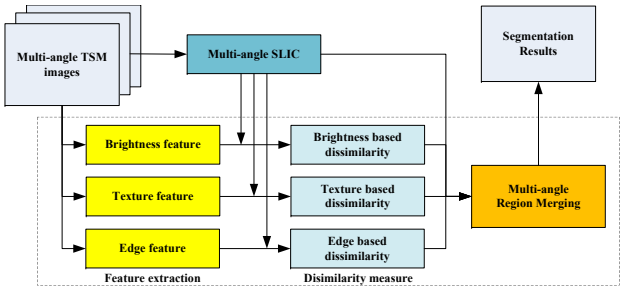

Fig. 2: Framework of the proposed method

$\mathbf{x}_p = \{l_p, a_p, b_p, x_p, y_p\}$, where l_p, a_p and b_p are l, a, and b components of the pixel p in CIELAB color space, x_p and y_p are x- and y-coordinate of p. In this paper, the image to be segmented is multi-angle TSM images, which are represented as $\vec{\mathbf{X}} = \{\mathbf{X}^m\}_{m=1}^M$, where $\mathbf{X}^m = \{\mathbf{x}_p^m\}_{p\in P}$ denotes the image of the m-th angle and M is the total number of angles.

2.2. Multi-angle SLIC

SLIC [11] is a segmentation method which can produce nearly uniform and boundary coherent superpixels for an input image. The distance $Dist_{p,q}$ between two pixels p and q is measured in both color and spatial space, which is defined as

$$\begin{aligned} Dist_{p,q} =& \sqrt{(l_p - l_q)^2 + (a_p - a_q)^2 + (b_p - b_q)^2} \\ &+ \frac{\gamma}{H}\sqrt{(x_p - x_q)^2 + (y_p - y_q)^2} \end{aligned} \tag{1}$$

where γ is a control ratio balancing color and space proximity, $H = \sqrt{N/K}$, and K is the expected number of superpixels.

To improve SLIC, we define the clustering energy function according to Centroidal Voronoi Tessellation [12] as

$$E(W; V) = \sum_{i=1}^{K} \sum_{p\in V_i} Dist_{p,w_i} \tag{2}$$

where $V = \{V_i\}_{i=1}^K$ is called the Voronoi clustering, and $W = \{w_i\}_{i=1}^K$ is the set of centroids of the clusters. For M-angle images $\vec{\mathbf{X}}$, we have the set of multi-angle cluster centroid $\vec{W} = \{\vec{w_i} = \{w_i^m\}_{m=1}^M\}_{i=1}^K$. From Fig.1, it's easy to observe that one grain is visually distinct from adjacent grains in some angles while obscured by neighbors in other angles, hence we define the distance of two pixels in multi-angle images to be the max value among all angles.

$$Dist_{\vec{p},\vec{q}} = \max_k Dist_{p^k,q^k} \tag{3}$$

where $\vec{p} = \{p^m\}_{m=1}^M$ is the pixel vector for p computed from M-angle images, and $\vec{q}$ likewise. Combining Eq.2 and Eq.3, we get the following multi-angle energy function which should be minimized after segmentation.

$$E(\vec{W}; V) = \sum_{i=1}^{K} \sum_{p\in V_i} Dist_{\vec{p},\vec{w_i}} \tag{4}$$

Algorithm 1 Multi-angle SLIC (MSLIC)

Input: $\vec{\mathbf{X}}$, the M-angle images
K, the expected number of superpixels
Output: V, the initial segmentation results of $\vec{\mathbf{X}}$
1: Initialize clusters V and cluster centers $\vec{w}$
2: Compute the optimal w^* by minimizing Eq.4
3: **repeat**
4: **for** each cluster center w_i^* **do**
5: **for** each pixel p in $2H \times 2H$ square around w_i^* **do**
6: Assign p to the best matching cluster V_i
7: **end for**
8: **end for**
9: Compute new cluster centers w' by minimizing Eq.4
10: Compute residual error $R = \|w^* - w'\|_2$
11: Set $w^* = w'$
12:**until** $R \leqslant$ threshold

The multi-angle SLIC (MSLIC) is described in Algorithm 1. In line 10, the residual error R is computed by a L_2 norm.

2.3. Feature Extraction and Dissimilarity Measure

In order to measure the dissimilarity between two superpixels, heterogeneous and complementary features are required to describe the distinct characteristics of the mineral grains.

One important and commonly used feature is brightness, denoted as f_p^B. The f_p^B is a pixel-level feature, the brightness feature for a superpixel V_i is defined as

$$sf_i^B = \frac{\sum_{p\in V_i} f_p^B}{|V_i|} \tag{5}$$

where $|\cdot|$ denotes the cardinality of the set. Then the brightness based dissimilarity between V_i and V_j is given by

$$DSim_{ij}^B = \|sf_i^B - sf_j^B\|_1 \tag{6}$$

where $\|\cdot\|_1$ stands for the 1-norm distance.

Another important feature is texture, which can characterize the structure of minerals. In this paper, gabor filter bank [13] is used to compute the texture feature $\mathbf{f}_p^T = \{f_p^T(i)\}_{i=1}^{N_\omega \times N_\theta}$, where N_ω and N_θ denote the number of frequencies and orientations of the gabor filter bank respectively. For superpixel V_i, its texture feature is defined as

$$\mathbf{sf}_i^T = \frac{\sum_{p\in V_i} \mathbf{f}_p^T}{|V_i|} \tag{7}$$

The texture based dissimilarity is given by

$$\begin{aligned} DSim_{ij}^T = \min\Big(&\sum_{k=1}^{N_\omega \times N_\theta} \frac{(sf_i^T(k) - sf_j^T(k))^2}{sf_i^T(k)}, \\ &\sum_{k=1}^{N_\omega \times N_\theta} \frac{(sf_i^T(k) - sf_j^T(k))^2}{sf_j^T(k)}\Big) \end{aligned} \tag{8}$$

where $sf_i^T(k)$ denotes the k-th value of $\mathbf{sf}_i^T$. Here we choose $\theta \in \{0, \pi/6, \pi/3, \pi/2, 2\pi/3, 5\pi/6\}$ and $\omega \in \{0.1, 0.3, 0.6, 0.8\}$.

The third important feature is the edges between adjacent superpixels. In this paper, a rotation invariant scharr filter [14] is used for edge feature extraction. For pixel p, it is convolved with the scharr kernel to obtain its edge feature f_p^E. The edge based dissimilarity between superpixels V_i and V_j is given by

$$DSim_{ij}^E = \frac{\sum_{k \in C(V_i, V_j)} f_k^E}{|C(V_i, V_j)|} \tag{9}$$

where $C(V_i, V_j)$ represents the pixels on the edges between superpixel V_i and V_j.

So far, we have defined the dissimilarities between adjacent superpixels based on brightness, texture and edge features. After scaling each of the three measures to range [0,1], the final combined dissimilarity is computed as

$$DSim_{ij} = DSim_{ij}^B + DSim_{ij}^T + DSim_{ij}^E \tag{10}$$

2.4. Multi-angle Region Merging

After MSLIC, the resulted neighboring superpixels should be further merged to yield a meaningful grain. For this purpose, we use the region adjacency graph (RAG) [15], which is an undirected graph $G = (V, L)$ corresponding to the *K*-partition image, where V is the set of nodes and L is the set of links. Each superpixel is represented as a graph node and there is a link l_{ij} between any two adjacent superpixels V_i and V_j. A cost $\delta(V_i, V_j)$ is assigned to each link to express the dissimilarity between adjacent superpixels, which is defined as

$$\delta(V_i, V_j) = \vec{DSim}_{ij} = \max_m DSim_{ij}^m \tag{11}$$

Algorithm 2 Multi-angle Region Merging (MRM)

Input: $\vec{\mathbf{X}}$, the *M*-angle images
V, the initial segmentation of $\vec{\mathbf{X}}$
Output: V_{final}, the final segmentation result
1: Construct RAG $G^0 = (V^0, L^0)$ according to $\vec{\mathbf{X}}$ and V
2: Set $t = 0$
3: **repeat**
4: Find the minimal cost link l_{ij} in G^t
5: Merge superpixel V_i and V_j
6: $t = t + 1$
7: Reconstruct G^t
8: Compute $F(t)$ according to Eq.12
9: **until** L^t is empty
10:Set $V_{final} = V^{opt}$, s.t. $opt = \underset{t}{\operatorname{argmax}} F(t)$

The merging is an iterative process (Algorithm 2), however, the stop criteria for merging is difficult to determine. In this paper, we define a function to describe the profit after each merging. Suppose that $G^t = \{V^t, L^t\}$ is the RAG after *t*-th merging, where $V^t = \{V_i^t\}_{i=1}^{K-t}$, $l_{ij}^t \in L^t, i \neq j, i, j = 1, 2, \cdots, K-t$, and V^0 is the initial segmentation result after MSLIC. we define the profit function after *t*-th merging as

$$F(t) = \frac{Intra(t)}{Inter(t)} \tag{12}$$

where $Intra(t)$ and $Inter(t)$ are intra-region homogeneity and inter-region heterogeneity respectively. We define

$$Intra(t) = \sum_{k=1}^{K-t} \frac{\sum_{V_i^0, V_j^0 \in V_i^t} DSim_{ij}}{|V_k^t|} \tag{13}$$

where $|V_k^t|$ is the number of adjacent superpixels in V^0 which have been merged into V_k^t. And $Inter(t)$ is defined as

$$Inter(t) = \frac{\sum_{l_{ij}^t \in E^t} DSim_{ij}}{K - t} \tag{14}$$

It is noticed that at first both $Intra(t)$ and $Inter(t)$ gradually increase while adjacent superpixels are being merged. The profitable increasement will stop at some optimal point, after that a notable decline will occur with successive merging. Hence, the optimal segmentation of TSM images is the one which maximizes the profit function defined in Eq.12.

3. EXPERIMENTS

In this section, we begin with introducing the prepared TSM images. Then, the parameter settings of the proposed method are discussed. Finally, we report the experimental results including comparisons with other state-of-the-art methods.

3.1. The Image Database

We made the TSM images by a digital camera installed on a polarizer microscope with rotation stage under cross-polarized light. The automated rotating polarizing stage allows the thin section to remain fixed while the polarizers are rotated. The sampling procedure rotates the polarizers from 0° to 45° in 15° increments under cross-polarized light so that each thin section will produce 4-angle images. Each image has a resolution of 800×600 pixels.

3.2. Parameter Settings

The commonly used metrics for evaluating the performance of segmentation algorithms are precision, recall and *F*-measure [16]. In order to explore the influence of parameter settings on MSLIC, we carry out the experiments by varying both K and γ. Fig.3 (a)-(d) plot the trends of recall, precision and *F*-measure on γ. With the growth of γ, the recall is gradually decreased and the precision is gradually increased, the *F*-measure reaches the max value at $\gamma = 10$ in most cases. Fig.3 (e)-(h) plot the trends of recall, precision and *F*-measure on K. All the measures start decreasing after $K = 300$. Based on Fig.3, we choose $K = 300$ and $\gamma = 10$.

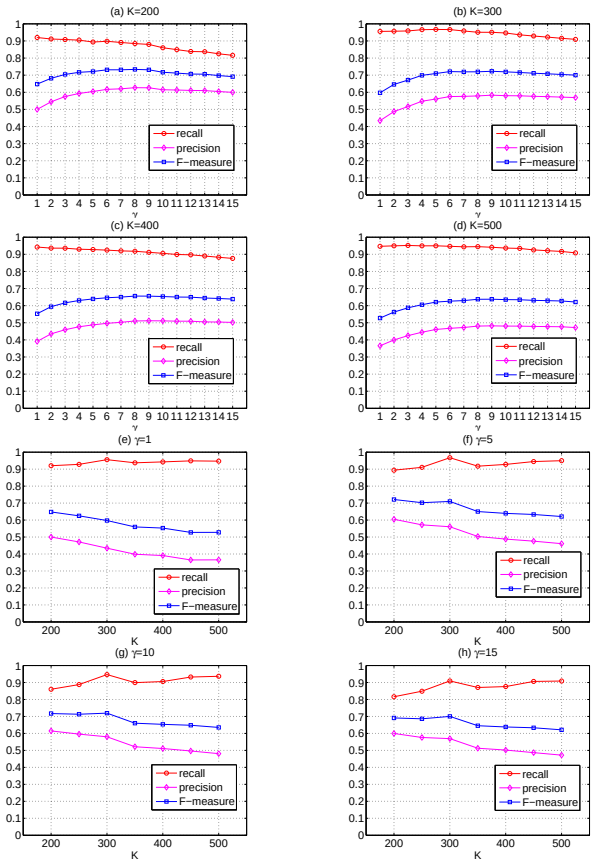

Fig. 3: The effects of parameter settings

3.3. Validation of MSLIC

To validate the effectiveness of the MSLIC algorithm, we compare it to seven state-of-the-art segmentation algorithms including FH[5], QS[6], TP[7], ERS[8], SEEDS[9], LSC[10] and SLIC[11]. The implementations of these algorithms are all publicly available. MSLIC works on multi-angle images and produce unique segmentation result. However, the competitive algorithms produce multiple results from multi-angle images. To make a fair comparison, we use the **maximum intensity image** [17][18] to get the best result for each of the seven algorithms. The results in columns (2)-(4) of Table 1 demonstrate that MSLIC outperforms the other competitive algorithms.

3.4. Validation of MRM

The strength of MRM algorithm is illustrated in Fig.4, of which (a) is the manual annotated ground truth, and (b) is the corresponding segmentation results by MRM. The experimental evidence suggests that MRM correctly merge the adjacent superpixels and get a favorable result. The columns (5)-(7) of Table 1 show that MRM could significantly improve precision and *F*-Measure with a slight decrease of recall.

Fig.5 explains the effectiveness of the stop criteria used in

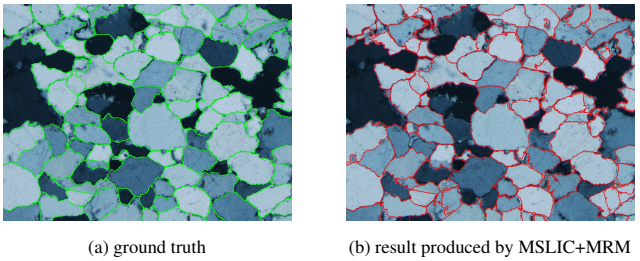

(a) ground truth (b) result produced by MSLIC+MRM

Fig. 4: Visual segmentation results

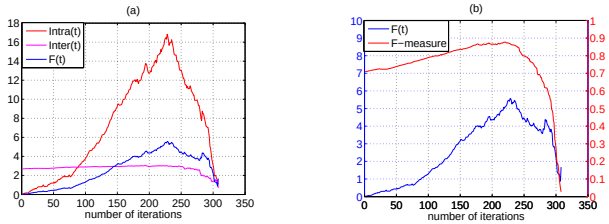

Fig. 5: Effectiveness of stop criteria for MRM

MRM. Fig.5 (a) shows that $Inter(t)$ increases slowly while $Intra(t)$ increases at a higher speed before the point of optimal merging. After that, both $Intra(t)$ and $Inter(t)$ decrease significantly which also decreases $F(t)$. Fig.5(b) illustrates that MRM makes optimal segmentation at maximum $F(t)$.

Table 1: Performance comparison among eight algorithms

	without MRM			with MRM		
	Precision	*Recall*	*F-Measure*	*Precision*	*Recall*	*F-Measure*
FH	0.5604	0.8148	0.6641	0.6360	0.7621	0.6934
QS	0.4798	0.8373	0.6100	0.7753	0.7827	0.7790
TP	0.4208	0.7835	0.5475	0.7532	0.7483	0.7507
ERS	0.5027	0.8816	0.6403	0.8106	0.8276	0.8190
SEEDS	0.4510	0.8196	0.5818	0.6363	0.7899	0.7048
LSC	0.5020	0.9157	0.6485	0.7403	0.8661	0.7982
SLIC	0.5204	0.9002	0.6596	0.6743	0.8451	0.7501
MSLIC	**0.5606**	**0.9672**	**0.7098**	**0.8406**	**0.9081**	**0.8730**

4. CONCLUSION

In this paper, we develop a method for segmentation of TSM images. The method consists of two steps: MSLIC and MRM. MSLIC makes use of multi-angle TSM images to get the initial superpixels, while MRM merges the adjacent superpixels to mineral grains. The experimental results demonstrate that the proposed method yield competitive results compared with state-of-the-art segmentation methods. In the future, we plan to improve the method by designing extra features [19] to describe the characteristics of TSM images, and adopt semantic segmentation [20][21] technologies to enhance the grain segmentation.

5. REFERENCES

[1] Pascal Asmussen, Olaf Conrad, Andreas Gnther, Moritz Kirsch, and Ulrich Riller, "Semi-automatic segmentation of petrographic thin section images using a seeded-region growing algorithm with an application to characterize wheathered subarkose sandstone," *Computers & Geosciences*, vol. 83, pp. 89–99, 2015.

[2] Simone Tarquini and Massimiliano Favalli, "A microscopic information system (mis) for petrographic analysis," *Computers & Geosciences*, vol. 36, no. 5, pp. 665–674, 2010.

[3] Hossein Izadi, Javad Sadri, and Nosrat-Agha Mehran, "A new intelligent method for minerals segmentation in thin sections based on a novel incremental color clustering," *Computers & Geosciences*, vol. 81, pp. 38–52, 2015.

[4] Matthias Jungmann, Hansgeorg Pape, Peter Wißkirchen, Christoph Clauser, and Thomas Berlage, "Segmentation of thin section images for grain size analysis using region competition and edge-weighted region merging," *Computers & Geosciences*, vol. 72, pp. 33–48, 2014.

[5] Pedro F Felzenszwalb and Daniel P Huttenlocher, "Efficient graph-based image segmentation," *International Journal of Computer Vision*, vol. 59, no. 2, pp. 167–181, 2004.

[6] Andrea Vedaldi and Stefano Soatto, "Quick shift and kernel methods for mode seeking," in *European Conference on Computer vision*, pp. 705–718. Springer, 2008.

[7] Alex Levinshtein, Adrian Stere, Kiriakos N Kutulakos, David J Fleet, Sven J Dickinson, and Kaleem Siddiqi, "Turbopixels: Fast superpixels using geometric flows," *IEEE Trans. on Pattern Analysis and Machine Intelligence*, vol. 31, no. 12, pp. 2290–2297, 2009.

[8] Ming Yu Liu, O. Tuzel, S. Ramalingam, and R. Chellappa, "Entropy rate superpixel segmentation," in *IEEE Conference on Computer Vision and Pattern Recognition*, 2011, pp. 2097–2104.

[9] Michael Van Den Bergh, Xavier Boix, Gemma Roig, and Luc Van Gool, "Seeds: Superpixels extracted via energy-driven sampling," *International Journal of Computer Vision*, vol. 111, no. 3, pp. 298–314, 2015.

[10] Zhengqin Li and Jiansheng Chen, "Superpixel segmentation using linear spectral clustering," in *IEEE Conference on Computer Vision and Pattern Recognition*, 2015, pp. 1356–1363.

[11] Radhakrishna Achanta, Appu Shaji, Kevin Smith, Aurelien Lucchi, Pascal Fua, and Sabine Susstrunk, "Slic superpixels compared to state-of-the-art superpixel methods," *IEEE Trans. on Pattern Analysis and Machine Intelligence*, vol. 34, no. 11, pp. 2274–2282, 2012.

[12] Jie Wang, Lili Ju, and Xiaoqiang Wang, "An edge-weighted centroidal voronoi tessellation model for image segmentation," *IEEE Trans. on Image Processing*, vol. 18, no. 8, pp. 1844–1858, 2009.

[13] Cheng Yaw Low, Beng Jin Teoh, and Cong Jie Ng, "Multi-fold gabor filter convolution descriptor for face recognition," in *IEEE International Conference on Acoustics, Speech and Signal Processing*, 2016, pp. 2094–2098.

[14] Bernd Jahne, Peter Geissler, and Horst Haussecker, *Handbook of Computer Vision and Applications*, Academic Press, New York, 1999.

[15] M Guinin, Ruan Su, L Nkhali, and B Dubray, "Segmentation of pelvic organs at risk using superpixels and graph diffusion in prostate radiotherapy," in *IEEE International Symposium on Biomedical Imaging*, 2015, pp. 1564–1567.

[16] D. M. W. Powers and Ailab, "Evaluation: From precision, recall and f-measure to roc, informedness, markedness & correlation," *Journal of Machine Learning Technologies*, vol. 2, pp. 2229–3981, 2011.

[17] Frank Fueten and Jeffrey Mason, "An artificial neural net assisted approach to editing edges in petrographic images collected with the rotating polarizer stage," *Computers & Geosciences*, vol. 33, no. 9, pp. 1176–1188, 2007.

[18] N. Yesiloglu-Gultekin, A. S. Keceli, E. A. Sezer, A. B. Can, C. Gokceoglu, and H. Bayhan, "A computer program (tsecsoft) to determine mineral percentages using photographs obtained from thin sections," *Computers & Geosciences*, vol. 46, no. 3, pp. 310–316, 2012.

[19] Mircea Cimpoi, Subhransu Maji, and Andrea Vedaldi, "Deep filter banks for texture recognition and segmentation," in *IEEE Conference on Computer Vision and Pattern Recognition*, 2015, pp. 3828–3836.

[20] Jonathan Long, Evan Shelhamer, and Trevor Darrell, "Fully convolutional networks for semantic segmentation," in *IEEE Conference on Computer Vision and Pattern Recognition*, 2015, pp. 3431–3440.

[21] Joao Carreira, Caseiro Rui, Jorge Batista, and Cristian Sminchisescu, "Free-form region description with second-order pooling," *IEEE Trans. on Pattern Analysis & Machine Intelligence*, vol. 37, no. 6, pp. 1177–89, 2015.